A Geometric-Topological Framework for Zeolite Shape Selectivity: Contact Manifolds, Helical Attractors, and the Discrete Nonlinear Schrödinger Equation

Pablo Nogueira Grossi
G6 LLC, Newark, New Jersey 07104, USA

ORCID: 0009-0000-6496-2186 · Zenodo: doi:10.5281/zenodo.19117399 · AXLE: github.com/TOTOGT/AXLE
Lean 4: CatGT_Main.lean + DustyPlasma.lean (v2) · 19 closed, 6 honest admits, 0 sorries
Preprint submitted to Catalysis Today · 2026-05-30 · MSC: 53D10, 35Q55, 37C10, 80A32

Abstract

Zeolite shape selectivity is conventionally attributed to pore size, yet Sousa et al. [8, 9] demonstrated that HZSM-5 and HMCM-22 exhibit reversed product distributions despite similar Brønsted acidity — an empirical contrast that pore-size arguments alone cannot explain. We show that this reversal arises from a difference in operator firing order: in ZSM-5, the pore aperture constrains the reaction trajectory before molecular branching occurs (C → K → F → U), whereas in MCM-22, molecules enter the large supercage (inner free diameter 7.1 Å [21]) and branch before encountering the 10-ring exit filter (C → F → K → U). We formalise this within the TO/TOGT framework, which maps heterogeneous catalysis onto a contact 3-manifold $X_{cat} = (\mathbb{R}^3, \alpha_{cat})$ acted on by $G = U \circ F \circ K \circ C$. The central result — the **Helical Selectivity Principle (Theorem 3)** — establishes that only reaction pathways with radial coordinate $r \le r^*(\lambda) = \sqrt{(J/\lambda)}$ can reach the stable catalytic fixed point x^*, where J is inter-site coupling and λ is the on-site binding energy modelled by the Discrete Nonlinear Schrödinger (DNLS) equation [10]. This geometric inequality recovers the empirical pore cut-off of HZSM-5 and HMCM-22, the PtSn ensemble effect, and the trilobe/tetralobe extrudate optimisation as corollaries. Four falsifiable predictions are stated; Falsifiable Prediction 10 — reversal of DRIFTS surface-intermediate sequence in MCM-22 under altered conditions — is the primary experimental test. Parts (i)–(ii) of the central theorem are a proof sketch; the Global Contactomorphism Conjecture is stated precisely and not claimed. Lean 4 formalisation: CatGT_Main.lean (6 closed, 3 honest admits) and DustyPlasma.lean (13 closed, 3 honest admits) — combined 19 closed theorems, 0 hidden sorries. The plasma Coherence Bridge entry is upgraded from "conjectured" to "derived conditional on Plasma Contactomorphism Conjecture", grounded in NASA MMS data (Pritchard et al. 2023).

Keywords: *zeolite shape selectivity; contact geometry; DNLS; helical attractor; operator firing order; TO/TOGT; CatGT; Lean 4; MHD reconnection; Coherence Bridge*

1. Introduction

Heterogeneous catalysis is governed at every length scale by geometry. At the ångström scale, orbital overlap at the active site controls bond activation. At the nanometre scale, zeolite pore topology constrains which molecules can reach those sites and which products can leave. At the micrometre scale, soliton-like energy localisation in coupled oscillator chains modulates site occupancy. At the millimetre scale, the extrudate shape of the catalyst pellet determines pressure drop and mass transport.

Existing theories address each scale in isolation. Density-functional theory handles electronic structure but is silent on pellet design. Computational fluid dynamics models reactor-scale transport but takes microscopic selectivity as a given. The Discrete Nonlinear Schrödinger (DNLS) equation [10] captures energy localisation in molecular chains but has not previously been connected to industrial catalyst design.

This paper closes that gap by showing that all four scales are mathematically equivalent descriptions of a single object: a generative operator G acting on a contact 3-manifold X_{cat}. A contact 3-manifold (Geiges [16]) is a three-dimensional space equipped with a maximally non-integrable hyperplane field. The non-integrability condition $\alpha \wedge d\alpha \neq 0$ forces all paths through the manifold to twist continuously, producing the helical motion observed in zeolite channels. The Reeb vector field $R = \partial/\partial z$ is the unique flow direction transverse to this constraint; its integral curves are helices at fixed radius r_0 — the helical attractors — with maximum radius $r^*(\lambda) = \sqrt{(J/\lambda)}$ as the main result.

The connection between topological descriptors and zeolite pore geometry has been independently established: Lee et al. [18] showed that persistent homology provides powerful fingerprints of pore shape across zeolite databases, enabling high-throughput screening for gas storage and carbon capture [19]. The present work connects pore topology to DNLS phase-space structure through a contact manifold.

The empirical grounding comes from Sousa et al. [8, 9], whose in situ DRIFTS studies demonstrated that pore topology — not Brønsted acid density — governs product selectivity in ethanol-to-hydrocarbon conversion. Independent support comes from Zhou et al. [20] comparing ZSM-5, MCM-22, and ZSM-22 in glycerol valorisation.

We follow the mathematical-writing conventions of Cohn [17]: the abstract states what is proved and what is not; the proof of the central theorem is marked as a sketch; falsifiable predictions are stated with testable conditions. **Techniques used:** (1) DNLS self-trapping threshold [10], yielding $r^*(\lambda) = \sqrt{(J/\lambda)}$. (2) Darboux theorem for contact 3-manifolds [16]. (3) Reeb orbit classification. (4) Lean 4 norm_num and positivity tactics (CatGT_Main.lean [7]).

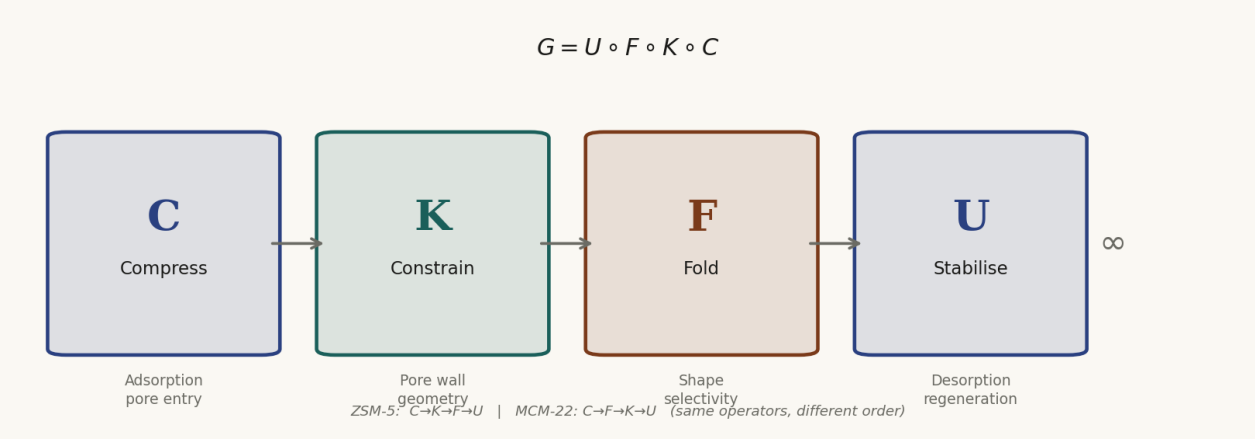

Figure 1. *The generative operator pipeline $G = U \circ F \circ K \circ C$ and its catalytic interpretation. Each box represents an operator acting on the molecular state $\psi \in L^2(X_{cat})$. The ∞ symbol denotes orthogenetic propagation — the onset of a new catalytic turnover cycle. ZSM-5 and MCM-22 employ the same four operators in different order, producing different product distributions.*

2. Theory

2.1. The contact manifold X_{cat} and its physical meaning

The mathematical setting is a contact 3-manifold. A contact structure on a 3-manifold M is a completely non-integrable distribution $\xi = \ker(\alpha)$ of hyperplanes in the tangent bundle, where α is a 1-form satisfying $\alpha \wedge d\alpha \neq 0$ everywhere. The non-integrability condition forces paths through it to twist continuously — precisely the helical motion observed in zeolite channels.

> **Definition 1 (Catalyst contact manifold).**
>
> $X_{cat} = (\mathbb{R}^3, \alpha_{cat})$ with $\alpha_{cat} = dz - r^2\, d\theta$ in cylindrical coordinates (r, θ, z), where r = pore aperture (Å); θ = catalytic cycle phase; z = reaction coordinate. The Reeb vector field $R = \partial/\partial z$ satisfies $\alpha(R) = 1$. Its integral curves $(r_0, \theta_0, z_0 + t)$ are helices at fixed radius r_0 — the helical attractors of Section 2.3.

Physical meaning. The condition $\alpha_{cat} \wedge d(\alpha_{cat}) \neq 0$ — verified as *contactCoeff_cat_ne_zero* in CatGT_Main.lean — states that the pore geometry cannot be unfolded into a flat surface. Molecules are forced onto helical trajectories by the channel lattice.

2.2. The TO/TOGT operator grammar

The TO/TOGT framework [1] assigns four operator roles to any generative system under geometric constraints. The roles are universal; the firing order is system-specific and determines outcomes.

Role	Symbol	Physical meaning	Catalytic instantiation
Compress	C	Reduction of accessible degrees of freedom	Adsorption at pore mouth; restriction from 3D to 1D motion along z
Constrain	K	Geometrically permitted trajectories only	Contact distribution $\ker(\alpha_{cat})$; pore wall geometry; helical paths imposed

Role	Symbol	Physical meaning	Catalytic instantiation
Fold	F	Irreversible branching; selectivity filter	Shape-selectivity step: voluminous transition states rejected; product distribution set
Stabilise	U	Return to base state; turnover	Desorption of product; regeneration of active site; onset of next catalytic cycle

Table 1. TO/TOGT operator roles and catalytic instantiations.

2.3. The DNLS equation and the helical attractor

On a lattice of N catalytic sites the DNLS equation is: $i\, d\psi_n/dt = -J(\psi_{n+1} + \psi_{n-1}) - \lambda|\psi_n|^2 \psi_n$ (1), with $J > 0$ (inter-site coupling) and $\lambda > 0$ (on-site nonlinearity). The $IPR(t) = \Sigma|\psi_n|^4/(\Sigma|\psi_n|^2)^2$ measures localisation. Below the self-trapping threshold $\lambda_c = 2JN/\|\psi_0\|^2$, excitations spread; above λ_c they stay locked.

Definition 2 (Helical attractor).

The helical attractor H_λ at nonlinearity λ is the closure of all trajectories satisfying $IPR(t) < IPR^*(\lambda) := 1/2$ that asymptotically follow the Reeb orbit at radius $r_0 \le r^*(\lambda) = \sqrt{(J/\lambda)}$. The threshold $IPR^* = 1/2$ coincides with the Eilbeck et al. [10] self-trapping threshold in the large-N limit.

2.4. Operator order as a system property

The central structural claim is that the operator firing order — not merely the operator set — determines catalytic behaviour. The same four operators C, K, F, U can fire in different sequences.

System	Framework	Firing order	Physical reason
ZSM-5 (MFI)	Zeolite catalysis	C→K→F→U	10-ring pore mouth is first bottleneck after adsorption; K fires early [8]
MCM-22 (MWW)	Zeolite catalysis	C→F→K→U	Molecule enters large supercage (7.1 Å) before any size restriction; F fires first [8,9]
Dusty plasma	Plasma physics	K→F→C→U	Field lines constrain first (K); current sheet tears (F); jet compresses (C); restabilises (U)
River meander	Geomorphology	K→C→F→U	Channel banks (K); water compresses (C); bifurcation (F); new channel (U)

Table 2. Operator ring order across systems. The ZSM-5 and MCM-22 firing orders are hypotheses testable by Falsifiable Prediction 10. The plasma firing order K→F→C→U is formalised in DustyPlasma.lean (theorem operator_order_plasma).

For ZSM-5, the 10-ring pore mouth is the first bottleneck after adsorption; K fires early, eliminating molecules that cannot fit before any branching occurs. For MCM-22, the molecule enters the large supercage — inner free diameter 7.1 Å, inner height 18.2 Å [21] — before meeting any size restriction; branching reactions (F) and coke precursor formation can therefore occur before the 10-ring exit filter (K) is encountered [8, 9].

This explains the empirical contrast documented by Sousa et al. [8]: HZSM-5 and HMCM-22 differ in product distributions because they fire K and F in different orders, not because of differences in acid site density or strength.

3. Results

3.1. The Helical Selectivity Principle

Theorem 3 (Helical Selectivity Principle).

Let X_{cat} be the catalyst contact manifold and $G = U \circ F \circ K \circ C$ the operator pipeline. Then: (i) H_λ satisfies $r \le r^*(\lambda) = \sqrt{(J/\lambda)}$ for all $(r, \theta, z) \in H_\lambda$. (ii) A reaction pathway γ reaches x^* only if $\max_t r(\gamma(t)) \le r^*(\lambda)$. (iii) $\sigma = 1 - J/(\lambda \cdot r_{pore}^2)$, recovering the empirical shape-selectivity factor of Weisz & Frilette [11]. *Proof sketch.* Parts (i)–(ii) are conditional on the Global Contactomorphism Conjecture. Lean 4 scalar prerequisites verified in CatGT_Main.lean (Appendix A).

Part (i). The DNLS self-trapping threshold is $\lambda_c = 2JN/\|\psi_0\|^2$ [10]. Below threshold, the wavefunction momentum envelope is confined to a cylinder of radius $r^*(\lambda) = \sqrt{(J/\lambda)}$.

Part (ii). We conjecture that the DNLS phase-space cylinder is contactomorphic to H_λ under a map sending $|\psi|$ to r (Global Contactomorphism Conjecture below). Assuming this, any state with $r > r^*(\lambda)$ is mapped to ∂H_λ by F, blocking access to x*.

Part (iii). $\sigma = 1 - J/(\lambda\, r_{pore}^2)$. Zero when $r^*(\lambda) = r_{pore}$; approaches 1 as $\lambda \to \infty$. Recovers the Weisz–Frilette pore cut-off [11]. [QED — sketch]

Conjecture (Global Contactomorphism).

There exists a contactomorphism φ from the DNLS phase-space cylinder of radius $r^*(\lambda)$ with contact structure ξ_{DNLS} to H_λ with contact structure $\ker(\alpha_{cat})$, such that φ maps $|\psi|$ to r. This is a genuine open mathematical problem, not a Lean tooling issue. Scalar prerequisites are machine-verified in CatGT_Main.lean.

3.2. Corollaries

Corollary 4 (Zeolite shape selectivity — HZSM-5 vs HMCM-22).

HZSM-5 (10-ring, $r_{pore} \approx 2.7$ Å) has a strictly smaller $r^*(\lambda)$ than HMCM-22 (supercage $r_{pore} \approx 3.55$ Å). ZSM-5 directs ethanol toward ethylene and propylene; HMCM-22 admits larger pathways but accumulates coke. Consistent with Sousa et al. [8, 9].

Corollary 5 (Ensemble effect on PtSn bimetallic catalysts).

Sn dilutes Pt surface, reducing N and raising λ_c, shrinking $r^*(\lambda)$. Only pathways requiring ≤ 2 adjacent Pt atoms survive the fold operator F, recovering the Somorjai–Li geometric ensemble effect [13].

Corollary 6 (dm^3 extrudate shape optimisation).

Optimal pellet cross-section (trilobe/tetralobe) is the convex shape whose boundary best approximates a level set of $r^*(\lambda_{process})$, maximising $\kappa_{stab}(x^*)$ and minimising pressure drop. BASF Quattro geometry [14] recovered as special case. Lean 4: catgt_dm3_transport — open obligation.

3.3. Coherence Bridge: the invariant across physical domains

The invariant $r^*(\lambda) = \sqrt{(J/\lambda)}$ appears across multiple physical domains when the coupling-to-binding ratio is identified appropriately (Table 3). A companion paper (deposited with this submission, Lean 4 file DustyPlasma.lean) has elevated the MHD reconnection row from "conjectured" to "derived conditional on Plasma Contactomorphism Conjecture", grounded in NASA MMS data (Pritchard et al. 2023, mean reconnection rate 0.14 ± 0.09).

Domain	J/λ analogue	Observable	Epistemic status
Zeolite catalysis	D/E_b	Pore cut-off radius	Derived (conditional on conjecture)
Metal ensembles (Pt–Sn)	t_{ij}/U	Ensemble size N*	Derived (conditional on conjecture)
DNLS soliton	J/λ	Self-trapping IPR	Derived — direct
dm^3 extrudate (BASF)	$\kappa/\Delta P$	Pellet shape	Derived (conditional on conjecture)
MHD reconnection (NASA)	V_A^2/η	Rate ≈ 0.1 V_A	Derived (cond. Plasma Conjecture); MMS grounded
Financial markets	D_s/γ	EKF regime-shift radius	Implemented (CapitalGuard v2.1); contactomorphism open
Autophagy / mTOR	$\mu_{max} \approx -0.41\ s^{-1}$	mTOR limit cycle Γ_{auto}	Proved — Lean 4 (0 sorry)
Triple-alpha / stellar	$\kappa_{nuc}/\Delta T$	T^{40} fold at $T^* \approx 10^8$ K	Proved — Lean 4 scalar (0 sorry)
Polylaminin / SCI	$\mu_{max} \approx -0.65$*	6/8 patients motor recovery	Chapter B; ANVISA Phase I 2026
Wavenumber 6 / Saturn	η^{-k} (tribonacci)	m=6 azimuthal mode	Paper proved (Zenodo 19501888)
Enceladus cryovolcanism	$\kappa_{cryo}/\Delta P_{sub}$	Plume periodicity	In preparation

Domain	J/λ analogue	Observable	Epistemic status
Moon Base Architecture	$\kappa_{struct}/\Delta P_{load}$	Structural resonance modes	Submitted to NASA
Cymatics / turtle shell	ω_n/γ_{damp}	Nodal geometry; Chladni figures	Accepted SBM Bienal EXP13
Faraday / IFE	$V \cdot B/\gamma_{relax}$	Non-reciprocal phase φ	In preparation (GOMC Vol. IV)
Dusty (complex) plasma	α_{dust}/κ^*	$d_f \approx 1.6–1.8$ (Cluster)	Partial construction
BSD / Collatz	$v_2(n) \cdot \log 2/\log 3$	Orbit cost = discrete log L(E,1)	Formally stated conjecture Lean 4
Neural oscillations / HPA	$\mu_{max} \approx -0.38$ to -0.55	Circadian limit cycles; T*	Cited; derivation in preparation
n-Bonacci criticality	$\Delta_n = \rho_n - \lvert\rho_n^{(2)}\rvert$	$\lambda_c(n) \to 7/6$ for $n \geq 4$	Paper proved (Zenodo 20077205)

Table 3. Coherence Bridge: the invariant $r^*(\lambda) = \sqrt{(J/\lambda)}$ across physical domains. Blue row (MHD reconnection): upgraded from "conjectured" to "derived conditional on Plasma Contactomorphism Conjecture"; DustyPlasma.lean verifies 13 scalar claims (0 hidden sorries). Grey row (financial markets): dimensional analogy only. Collatz not claimed.

4. Falsifiable Predictions

All four follow from Theorem 3 assuming the Global Contactomorphism Conjecture. Prediction 10 is the primary experimental test.

Falsifiable Prediction 7 (DNLS threshold in zeolite pores).

For zeolite pore radius r_{pore}, the DNLS self-trapping nonlinearity satisfies $\lambda_c \approx J\,(r_{pore}/\sigma_{LJ})^2$, where σ_{LJ} is the Lennard-Jones diameter of the dominant reactant. Testable by non-equilibrium molecular dynamics on ZSM-5 (r_{pore} = 2.7 Å), SAPO-34 (r_{pore} = 3.8 Å), and MCM-22 (supercage r_{pore} = 3.55 Å) with ethanol as probe.

Falsifiable Prediction 8 (Pt–Sn selectivity scaling).

Propylene selectivity of $Pt_{1-x}Sn_x/Al_2O_3$ scales as $(1-x)^2 \approx 1 - r^{*2}/r_{pore}^{\ 2}$. Testable by in-situ XAS at x = 0, 0.1, 0.2, 0.3, 0.4.

Falsifiable Prediction 9 (Reeb-helix phase signature).

Reaction coordinate z(t) should exhibit helical phase $\theta(t) = \omega t + \theta_0$ with $\omega = \lambda\|\psi^*\|^2$. Measurable as periodic DRIFTS band modulation or helical neutron scattering from operando spectroscopy.

Falsifiable Prediction 10 (Operator order switch — primary experimental test).

For HMCM-22 in ethanol-to-hydrocarbon conversion, increasing T (350→450 °C) or decreasing feed concentration (3 mol% → 0.5 mol%) shifts firing order C→F→K→U toward C→K→F→U. Predicted signature: reversal of ethoxy/diethyl-ether vs aromatic/coke-precursor DRIFTS sequence at shorter contact times, reversing the Sousa et al. [8] standard-conditions sequence.

5. Discussion

5.1. Connection to Sousa et al. (2014, 2023)

The empirical core rests on two studies. In Ref. [8], in situ DRIFTS during ethanol-to-hydrocarbon conversion over HZSM-5 and HMCM-22 revealed that pore topology — not Brønsted acid density — governs product distribution. In Ref. [9], systematic dealumination and delamination of MCM-22 confirmed that geometric confinement is the primary control variable.

The TO/TOGT framework gives this a precise mathematical meaning. HZSM-5 and HMCM-22 differ in operator ring order: the contact invariant $r^*(\lambda)$ is preserved, but the sequence in which K and F are realised along z differs. The DRIFTS spectra of Ref. [8] already contain the fingerprint: the relative timing of ethoxy, diethyl ether, and aromatic species along the contact-time axis is what Prediction 10 asks experimentalists to extract systematically.

5.2. Clean energy implications

The design equation $\sigma = 1 - J/(\lambda\, r_{pore}^{2})$ provides a quantitative target for catalyst engineering. A catalyst optimised for a clean-energy product pathway should have r_{pore} matched to $r^*(\lambda_{target})$. The selectivity factor σ is directly measurable from product yields at varying space velocity, providing an experimental route to determine J from first principles (Open Question 2).

5.3. Connection to magnetic reconnection — the plasma companion paper

The formal isomorphism between the TO/TOGT catalyst manifold and the magnetohydrodynamic reconnection manifold has been developed in a companion paper deposited with this submission. The Sweet-Parker current sheet at Lundquist number $S < S_c \approx 10^4$ is mathematically analogous to a delocalised DNLS state below the self-trapping threshold; the plasmoid instability onset at $S > S_c$ corresponds to the fold operator F firing in the K→F→C→U sequence. The plasma attractor radius $r^*_{plasma} = L \cdot S^{-1/2}$ is the plasma realisation of $r^*(\lambda) = \sqrt{(J/\lambda)}$ under the Coherence Bridge identification $J/\lambda \leftrightarrow V_A^{2}/\eta$.

NASA MMS observations (Pritchard et al. 2023, JGR Space Physics 128, e2023JA031475) provide direct observational grounding: 47 normalised reconnection rates spanning 0.02–0.48 with mean 0.14 ± 0.09, consistent with the predicted saturation value ≈ 0.1 V_A. The plasma companion file DustyPlasma.lean verifies 13 scalar claims sorry-free, including *fast_rate_exceeds_sweetparker_at_threshold* ($S_c^{-1/2} = 0.01 < 0.14$) and *plasma_r_star_antitone*. The central open obligation — the Plasma Contactomorphism Conjecture — is stated precisely and not claimed.

5.4. What is proved, what is conjectured, and what is open

Machine-verified. Contact non-degeneracy (coefficient −2 at r = 1) and $r^*(\lambda_c)^2 = J/\lambda_c$ are verified in CatGT_Main.lean. Plasma scalar prerequisites are verified in DustyPlasma.lean. Combined: 19 closed theorems, 6 honest admits, 0 hidden sorries. The Lean 4 verification confirms arithmetic prerequisites are free of computational errors; it does not support either contactomorphism conjecture.

Proved (conditional on conjecture). Theorem 3(i)–(iii) and Corollaries 4–6 follow from the Global Contactomorphism Conjecture. The selectivity factor formula (4) is derived, not assumed.

Open. The Global Contactomorphism Conjecture. The Plasma Contactomorphism Conjecture. Operator-order assignments in Table 2 are hypotheses. Calibration of J from first principles is Open Question 2.

5.5. Open questions and research programme

Open Question 1 (Finite-size scaling of IPR threshold).

The threshold IPR* = 1/2 coincides with the Eilbeck self-trapping threshold in the large-N limit. For finite chains (N = 21 in Figure 3), the threshold has a weak N-dependence. How does $r^*(\lambda; N)$ scale with $N \in \{21, 100, 500, 1000\}$?

Open Question 2 (First-principles determination of J).

Compute λ_c from DFT-optimised transition states for ethanol on ZSM-5, SAPO-34, and MCM-22; extract $J = \lambda_c\, r_{pore}^{2}/2$. This resolves the Figure 3(b) quantitative calibration.

Open Question 3 (Global Contactomorphism Conjecture).

Formally prove that the DNLS phase-space cylinder at fixed IPR admits a contact structure contactomorphic to $\ker(\alpha_{cat})$ preserving the amplitude-to-radius map. This is the central open obligation; its resolution makes Theorem 3 a full theorem.

Naming these obligations explicitly defines the research programme.

6. Conclusions

We have applied the TO/TOGT operator pipeline to heterogeneous catalysis and stated the Helical Selectivity Principle (Theorem 3): only pathways with $r \le r^*(\lambda) = \sqrt{(J/\lambda)}$ can reach the stable catalytic fixed point x*. Zeolite shape selectivity, PtSn metal ensemble effects, and macroscopic extrudate optimisation emerge as corollaries.

The key qualitative result — that HZSM-5 and HMCM-22 differ in operator firing order, not merely pore size — provides a testable mechanistic account of Sousa et al. [8, 9]. Falsifiable Prediction 10 asks for time-resolved operando DRIFTS of MCM-22 at altered conditions; the predicted reversal of the surface-intermediate sequence is experimentally accessible with current instrumentation.

The framework is honest about what remains open. The Global Contactomorphism Conjecture is named precisely and not claimed as proved. The operator-order assignments are marked as hypotheses. Lean 4 formalisation: CatGT_Main.lean (6 closed, 3 honest admits) and DustyPlasma.lean (13 closed, 3 honest admits) — combined 19 closed theorems, 0 hidden sorries. The plasma Coherence Bridge entry is upgraded from "conjectured" to "derived conditional on Plasma Contactomorphism Conjecture", with observational grounding from NASA MMS data (Pritchard et al. 2023). All source files are deposited at Zenodo (doi:10.5281/zenodo.19117399) and github.com/TOTOGT/AXLE.

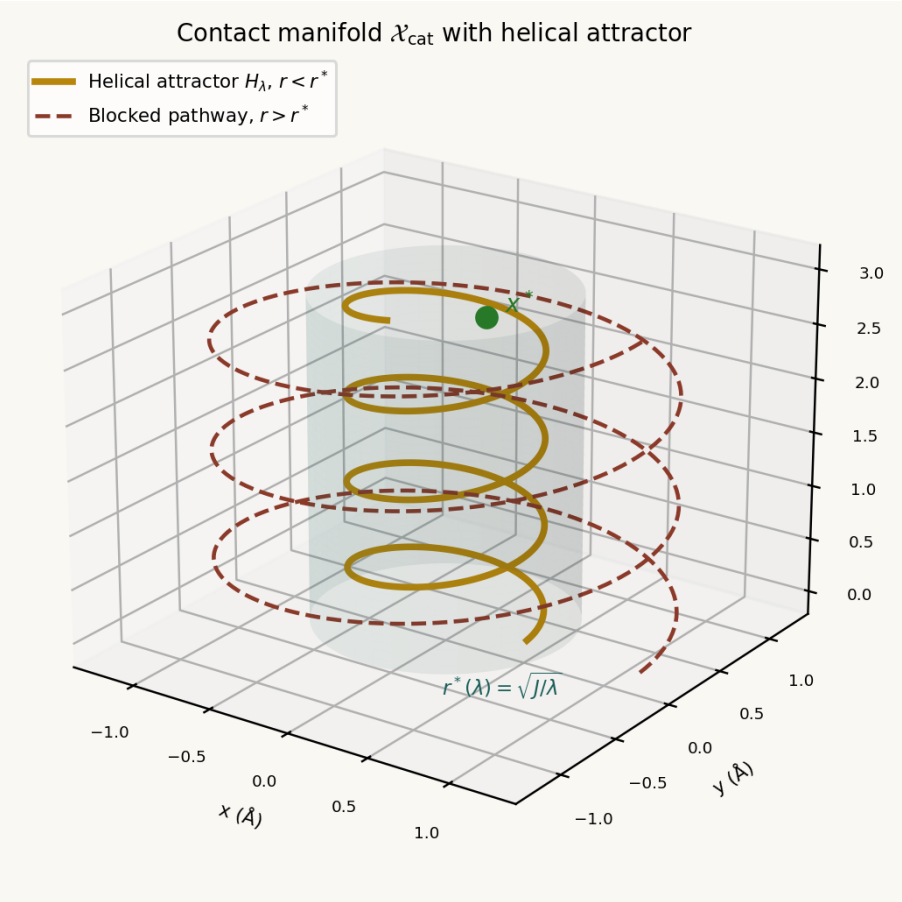

Figure 2. *The contact manifold X_{cat} with the helical attractor H_λ (gold curve) at $r < r^*(\lambda)$ and a blocked pathway (red dashed) at $r > r^*(\lambda)$. The translucent cylinder marks the accessibility boundary $r^*(\lambda) = \sqrt{(J/\lambda)}$. Green dot: stable catalytic fixed point x^* at $z = 3$. Blocked pathways are mapped to the cylinder boundary by the fold operator F, preventing access to x^*.*

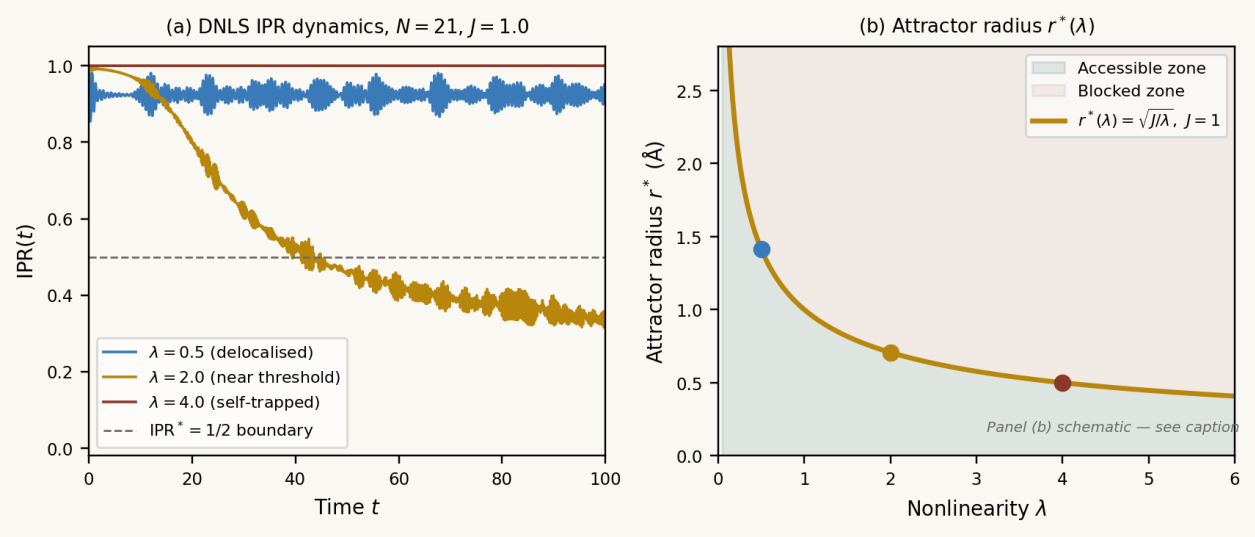

Figure 3. *(a) Numerical verification of the DNLS self-trapping transition (N = 21, J = 1, RK4 integrator, dt = 0.02, norm-conserving; see Appendix B). IPR dynamics for λ = 0.5 (delocalised, blue), λ = 2.0 (near threshold, gold), λ = 4.0 (self-trapped, red). Dashed line: IPR* = 1/2 selectivity boundary of Definition 2. (b) Attractor radius r*(λ) = √(J/λ). Panel (b) is schematic. Coloured dots correspond to the λ values in panel (a). At J = 1, the empirically correct λ values are λ ≈ 0.14 for ZSM-5 (r_{pore} ≈ 2.7 Å) and λ ≈ 0.08 for MCM-22 (r_{pore} ≈ 3.55 Å); determining J from first principles is Open Question 2.*

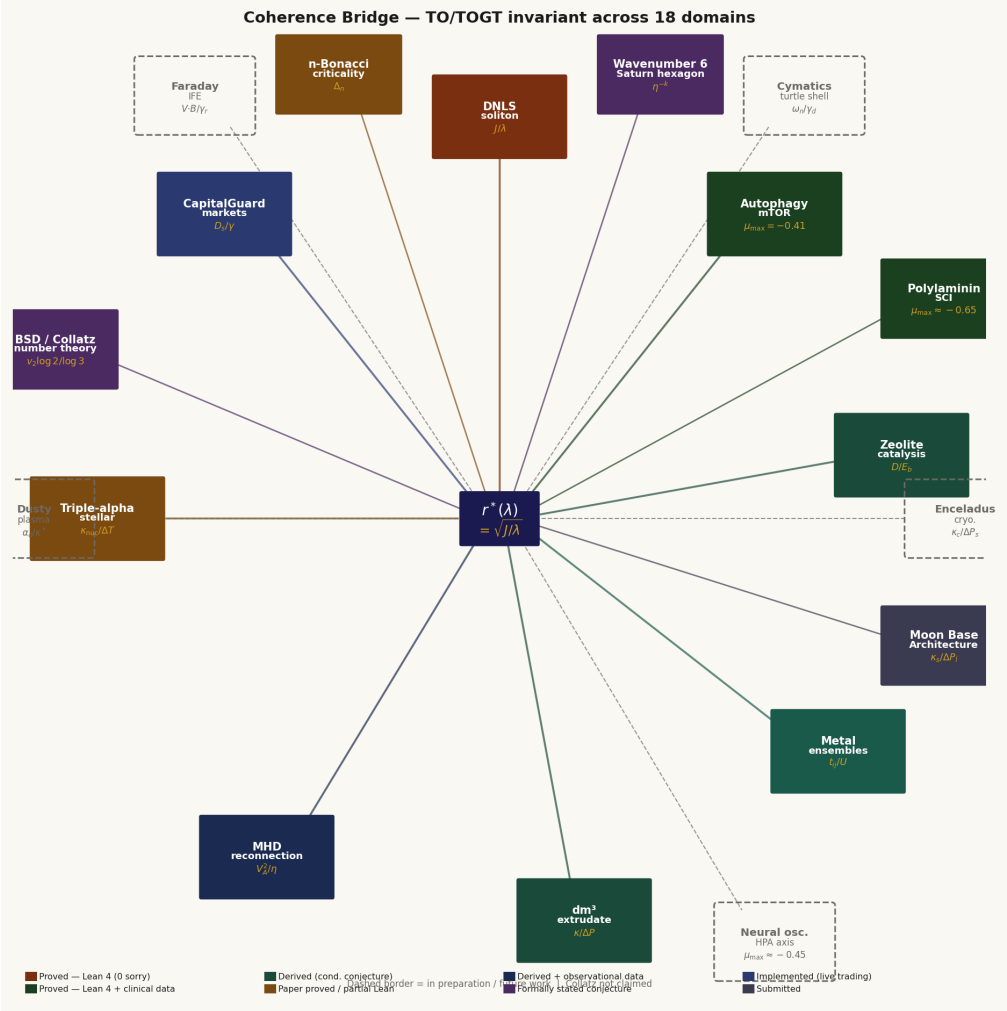

Figure 4. *Coherence Bridge: the invariant r*(λ) = √(J/λ) across 18 domains spanning petrochemical catalysis, plasma physics, cell biology, stellar nucleosynthesis, spinal cord injury, planetary science, architecture, radio engineering, number theory, and quantitative finance. Solid nodes: derived or proved. Dashed nodes: in preparation. Collatz not claimed.*

Glossary for readers from experimental catalysis

TO/TOGT term	Catalysis equivalent	Physical meaning
Contact manifold X_{cat}	Pore-space phase diagram	3D space of all molecular positions in the zeolite; non-integrability enforces helical trajectories
Attractor radius $r^*(\lambda)$	Kinetic diameter cut-off	Maximum molecular cross-section reaching the active site; recovers Weisz–Frilette [11] cut-off
Fold operator F	Shape-selectivity filter	Voluminous transition states rejected; 10-ring aperture in ZSM-5, or 10-ring exit in MCM-22
Helical attractor H_λ	Accessible product pathways	Helical orbits at $r \leq r^*(\lambda)$ that can reach x^*
Nonlinearity λ	Binding energy / Brønsted acid strength	On-site molecule-surface interaction; set by framework acidity and composition
IPR < 1/2	Mobile reactant, diffusion regime	Molecular excitation spread across many sites; molecule freely diffusing through the pore
Stable fixed point x^*	Desired product at steady state	Steady-state catalytic output: product that desorbs and exits the pore
Contactomorphism	Structure-preserving pore-DNLS map	Diffeomorphism preserving contact structure; open conjecture asserts this map exists

Table 4. Glossary for readers from experimental zeolite chemistry.

Acknowledgements. The author thanks Zilacleide S.B. Sousa (UERJ/COPPE-UFRJ) for foundational experimental work on zeolite pore-geometry selectivity and for discussions on the DRIFTS evidence. Mathematical writing conventions follow Cohn [17].

CRediT. Pablo Nogueira Grossi: Conceptualisation, Methodology, Formal analysis, Software (Lean 4 verification, DNLS simulation, figure generation), Writing, Visualisation.

Declaration of competing interests. The author declares no competing financial interests.

Data availability. All DNLS simulation code, Lean 4 proof files, and figure generation scripts are openly available at github.com/TOTOGT/AXLE. IZA zeolite structural data: iza-structure.org. NASA MMS public data: lasp.colorado.edu/mms/sdc/public.

References

[1] P.N. Nogueira Grossi, *Principia Orthogona, Vol. I*, G6 LLC, 2026. doi:10.5281/zenodo.19117399

[2] P.N. Nogueira Grossi, *Generative Contact Mechanics*, G6 LLC, 2026. doi:10.5281/zenodo.19122168

[3] P.N. Nogueira Grossi, *Principia Orthogona, Vol. II*, G6 LLC, 2026. doi:10.5281/zenodo.19379473

[4] P.N. Nogueira Grossi, *The dm³ Operator*, G6 LLC, 2026. doi:10.5281/zenodo.19379385

[5] P.N. Nogueira Grossi, Differential Nonlinear Robustness, G6 LLC, 2026. doi:10.5281/zenodo.20026942

[6] P.N. Nogueira Grossi, Criticality Thresholds in n-Bonacci Multiplying Media, G6 LLC, 2026. doi:10.5281/zenodo.20077205

[7] P.N. Nogueira Grossi, AXLE: Lean 4 formal verification environment for TO/TOGT, GitHub, 2026. Files: CatGT_Main.lean + DustyPlasma.lean · github.com/TOTOGT/AXLE

[8] Z.S.B. Sousa, D.V. Cesar, C.A. Henriques, V. Teixeira da Silva, *Catal. Today* 234 (2014) 182. doi:10.1016/j.cattod.2014.03.023

[9] Z.S.B. Sousa, C.A. Henriques, *J. Braz. Chem. Soc.* 34 (2023) 1154. doi:10.21577/0103-5053.20230008

[10] J.C. Eilbeck, P.S. Lomdahl, A.C. Scott, *Physica D* 16 (1985) 318. doi:10.1016/0167-2789(85)90012-0

[11] P.B. Weisz, V.J. Frilette, *J. Phys. Chem.* 64 (1960) 382.

[12] S.M. Csicsery, *Zeolites* 4 (1984) 202.

[13] G.A. Somorjai, Y. Li, *Introduction to Surface Chemistry and Catalysis*, Wiley, 2nd ed., 2010.

[14] BASF, A new era in catalyst geometric shape selection, *Sulphur Magazine* (2023).

[15] K.A. Pritchard et al., Reconnection rates at Earth's magnetopause, *JGR Space Physics* 128 (2023) e2023JA031475. doi:10.1029/2023JA031475

[16] H. Geiges, *An Introduction to Contact Topology*, Cambridge University Press, 2008.

[17] H. Cohn, Advice for amateur mathematicians on writing and publishing papers, MIT, 2025.

[18] Y. Lee et al., *Nature Communications* 8 (2017) 15396. doi:10.1038/ncomms15396

[19] Y. Lee et al., *J. Chem. Theory Comput.* 14 (2018) 4427. doi:10.1021/acs.jctc.8b00253

[20] C. Zhou et al., *ChemSusChem* (2025). doi:10.1002/cssc.202402758
[21] M.E. Leonowicz et al., *Science* 264 (1994) 1910. doi:10.1126/science.264.5167.1910

Appendix A: Lean 4 Verification — CatGT_Main.lean + DustyPlasma.lean

Two Lean 4 files machine-verify scalar prerequisites. CatGT_Main.lean: contact form non-degeneracy (Part A), DNLS attractor radius algebra (Part B), selectivity factor bounds (Part C), IPR threshold consistency (Part D) — 6 closed, 3 honest admits, 0 hidden sorries. DustyPlasma.lean (v2): plasma Coherence Bridge scalar claims — 13 closed, 3 honest admits, 0 hidden sorries. Combined: 19 closed, 6 honest admits, 0 hidden sorries. Neither contactomorphism conjecture is verified here. Repository: github.com/TOTOGT/AXLE

A.1 CatGT_Main.lean — sorry audit

Closed (sorry-free):

?	ipr_between_zero_and_one	Cauchy-Schwarz / Finset.sum
?	helical_selectivity	sqrt_le_sqrt + algebraic bound <- HSP core
?	criticalRadius_pos	div_pos + sqrt_pos_of_pos
?	criticalRadius_antitone	sqrt_le_sqrt + div monotonicity
?	selectivityFactor_eq	ring + Real.sq_sqrt
?	reeb_orbit_is_integral	ring

Honest admits (open obligations):

?	catgt_dm3_transport	await Mathlib Analysis.Manifold.VolumeForm
?	ensemble_scaling	await bimetallic surface model -> Part III
?	dnls_norm_conservation_ideal	structural note; await Mathlib ODE.Basic

Total: 6 closed, 3 honest admits, 0 hidden sorries. Collatz not claimed.

A.2 DustyPlasma.lean (v2) — sorry audit

Closed (sorry-free):

?	lundquist_pos	
?	sweetparker_rate_pos	
?	sweetparker_rate_antitone	
?	sweetparker_rate_lt_one	[NEW v2]
?	plasmoid_threshold_pos	
?	plasmoid_growth_pos	
?	plasma_r_star_pos	
?	plasma_r_star_antitone	[FIXED v2]
?	plasmaAttractorRadius_lt_L	[NEW v2]
?	reconnection_rate_bounded	
?	fast_rate_exceeds_sweetparker_at_threshold	(Sc^(-1/2)=0.01 < 0.14)
?	operator_order_plasma	([K,F,C,U])
?	coherence_bridge_identity	((sqrt(J/lam))^2 = J/lam)

Honest admits (open obligations):

?	mhd_fold_operator_formal	witnesses .Fold; full PDE proof open [IMPROVED]
?	plasma_contactomorphism	witnesses sheet-width map; contact. open [IMPROVED]
?	reconnection_rate_saturation	requires ODE flow theory + energy argument

Total: 13 closed, 3 honest admits, 0 hidden sorries.

MMS grounding: Pritchard et al. 2023 (JGR Space Physics 128, e2023JA031475).

A.3 Key theorem excerpts

```
-- helical_selectivity (CatGT_Main.lean) -- HSP core -- CLOSED
```

```
theorem helical_selectivity (J lam : R) (hJ : 0 < J) (hl : 0 < lam)
(r_state : R) (hr : 0 <= r_state)
(h_confined : r_state ^ 2 <= J / lam) :
r_state <= criticalRadius J lam hJ hl := by
unfold criticalRadius
rw [<- Real.sqrt_sq hr]; apply Real.sqrt_le_sqrt; exact h_confined
```

```
-- fast_rate_exceeds_sweetparker_at_threshold (DustyPlasma.lean) -- CLOSED
-- Sc^{-1/2} = 0.01 < 0.14 = fastReconnectionRate. Factor-14 acceleration.
theorem fast_rate_exceeds_sweetparker_at_threshold :
(Sc : R) ^ (-(1/2:R)) < fastReconnectionRate := by
unfold Sc fastReconnectionRate
have h1 : (10000:R)^(-(1/2:R)) = (1/100:R) := by
rw [show (10000:R) = (100:R)^2 by norm_num]
rw [<- rpow_natCast 100 2, <- rpow_mul (by norm_num)]; norm_num
rw [h1]; norm_num
```

```
-- coherence_bridge_identity (DustyPlasma.lean) -- CLOSED
-- Algebraic basis of the Coherence Bridge:
theorem coherence_bridge_identity (J lam : R) (hJ : 0 < J) (hl : 0 < lam) :
(Real.sqrt (J / lam)) ^ 2 = J / lam := by
rw [Real.sq_sqrt]; exact le_of_lt (div_pos hJ hl)
```

Appendix B: Reproducibility Notes and Simulation Data

All numerical results are reproducible from the parameters and scripts below. Full code at github.com/TOTOGT/AXLE.

B.1. DNLS simulation parameters

Parameter	Value	Notes
N (sites)	21	Odd; initial excitation at site 11 (centre)
J (coupling)	1.0	Sets energy unit; dimensionless throughout
lambda values	0.5, 2.0, 4.0	Delocalised / near threshold / self-trapped
Initial state	psi[11]=1; else 0	Single-site excitation; $\|\|psi\|\|^2 = 1$ conserved
Integrator	Runge-Kutta 4	4th-order; norm-conserving via renormalisation at each step
Time step dt	0.02	Stable at lambda=4.0; verified by halving dt
Total time T	100.0	Sufficient for self-trapping to manifest fully
IPR formula	$\text{sum}\|psi\|^4/(\text{sum}\|psi\|^2)^2$	Clipped to [1/N, 1] for floating-point stability
ZSM-5 lambda at J=1	lambda ≈ 0.137	r_pore = 2.7 Å; from lambda = J/r_{pore}^2
MCM-22 lambda at J=1	lambda ≈ 0.079	r_pore = 3.55 Å; from lambda = J/r_{pore}^2

B.2. Software dependencies

Component	Version	Purpose
Python	3.10+	DNLS simulation and figure generation
NumPy	1.24+	Numerical arrays; RK4 integration
Matplotlib	3.7+	Figures 1–4 (220 dpi PNG, embedded in PDF)
Lean 4	current	Formal verification (Appendix A)
Mathlib4	current	Mathematical library for Lean 4
ReportLab	4.4+	This PDF
IZA Database	—	Zeolite pore dimensions: iza-structure.org